Cell Host & Microbe
Article

A Murid Gamma-Herpesviruses Exploits Normal Splenic Immune Communication Routes for Systemic Spread

Bruno Frederico,[1] Brittany Chao,[1] Janet S. May,[1] Gabrielle T. Belz,[2] and Philip G. Stevenson[1,3,*]
[1]Division of Virology, Department of Pathology, University of Cambridge, Cambridge CB2 2QQ, UK
[2]Molecular Immunology, Walter and Eliza Hall Institute of Medical Research, Melbourne, Victoria 3052, Australia
[3]Sir Albert Sakzewski Virus Research Centre and Queensland Children's Medical Research Institute, University of Queensland, Brisbane, Queensland 4029, Australia
*Correspondence: p.stevenson@uq.edu.au
http://dx.doi.org/10.1016/j.chom.2014.03.010

SUMMARY

Gamma-herpesviruses (γHVs) are widespread oncogenic pathogens that chronically infect circulating lymphocytes. How they subvert the immune check-point function of the spleen to promote persistent infection is not clear. We show that Murid Herpesvirus-4 (MuHV-4) enters the spleen by infecting marginal zone (MZ) macrophages, which provided a conduit to MZ B cells. Relocation of MZ B cells to the white pulp allowed virus transfer to follicular dendritic cells. From here the virus reached germinal center B cells to establish persistent infection. Mice lacking MZ B cells, or treated with a sphingosine-1-phosphate receptor agonist to dislocate them, were protected against MuHV-4 colonization. MuHV-4 lacking ORF27, which encodes a glycoprotein necessary for efficient intercellular spread, could infect MZ macrophages but was impaired in long-term infection. Thus, MuHV-4, a γHV, exploits normal immune communication routes to spread by serial lymphoid/myeloid exchange.

INTRODUCTION

The γHVs persist in lymphocytes and cause lymphoid cancers. However, we know little about how lymphoid infection is established, because this precedes clinical presentation. In vitro Epstein-Barr virus (EBV) transforms primary B cells. However, in vivo it is found mainly in germinal center (GC)-derived resting memory B cells (Thorley-Lawson et al., 2008), arguing that infection is tightly linked to host functions. The involvement of other cell types is suggested by EBV colonizing epithelial, NK, and T cell cancers (George et al., 2012). The Kaposi's sarcoma-associated herpesvirus (KSHV) also infects a range of cell types (Ganem, 2006). Thus, B cell transformation may not reflect the full complexity of host colonization.

Analyses of EBV and KSHV are hampered by their narrow species tropisms. MuHV-4 (Nash and Sunil-Chandra, 1994; Blackman and Flaño, 2002; Stevenson et al., 2009; Barton et al., 2011), which is genetically similar to KSHV, provides a more tractable experimental route to understanding how γHVs establish chronic infection. Like EBV, it drives B cell proliferation in splenic GCs and persists in memory B cells. MuHV-4 enters new hosts via the olfactory neuroepithelium (Milho et al., 2012) or genital tract (François et al., 2013), dendritic cells (DCs) take it to lymph nodes (LNs) (Gaspar et al., 2011), and from there it reaches the spleen. The spleen normally limits vascular pathogen spread, so its infection is a key event in host colonization. Intranasal (i.n.) MuHV-4 requires B cells to reach the spleen (Usherwood et al., 1996). However, once there it infects newly formed, marginal zone (MZ) and GC B cells (Marques et al., 2003), which are unlikely to derive from LN memory B cells. Therefore, B cell recirculation and proliferation do not explain all the features of splenic infection.

Here we show that MuHV-4 enters the spleen by infecting MZ macrophages. It then reached MZ B cells. These relocated to the white pulp (WP) and transferred virions to follicular DCs. Infected B cells then appeared in WP GCs. These data establish a paradigm of γHV spread along immune communication pathways and suggest that targeting intercellular exchanges could help to limit chronic infection.

RESULTS

MuHV-4 Transits from LN to Spleen via a lysM$^+$ Cell

Inserting loxP sites into herpesvirus genomes can reveal their passage history by recombination in cre transgenic mice (Sacher et al., 2008). Applying this technique to MuHV-4 identified a role for CD11c$^+$ cells in LN colonization but not subsequent spread to the spleen (Gaspar et al., 2011). In lysM-cre mice, which express cre recombinase mainly in mature macrophages and granulocytes (Clausen et al., 1999), the same floxed virus (MHV-loxP-eCFP) showed minimal recombination in LN after 10 days and significant recombination in the spleen but not LN after 14 days (Figure 1A). Thus, lysM^{hi} cells played little role in virus passage to LN but a significant role in passage from LN to spleen. After 17 days recombination was also seen in LN, presumably reflecting splenic B cell recirculation, as by this time there is generalized lympadenopathy.

The loxP sites of MHV-loxP-eCFP incorporate a mutated spacer region that CD11c-cre mice recombine with only modest efficiency (Gaspar et al., 2011), and the low cre expression of

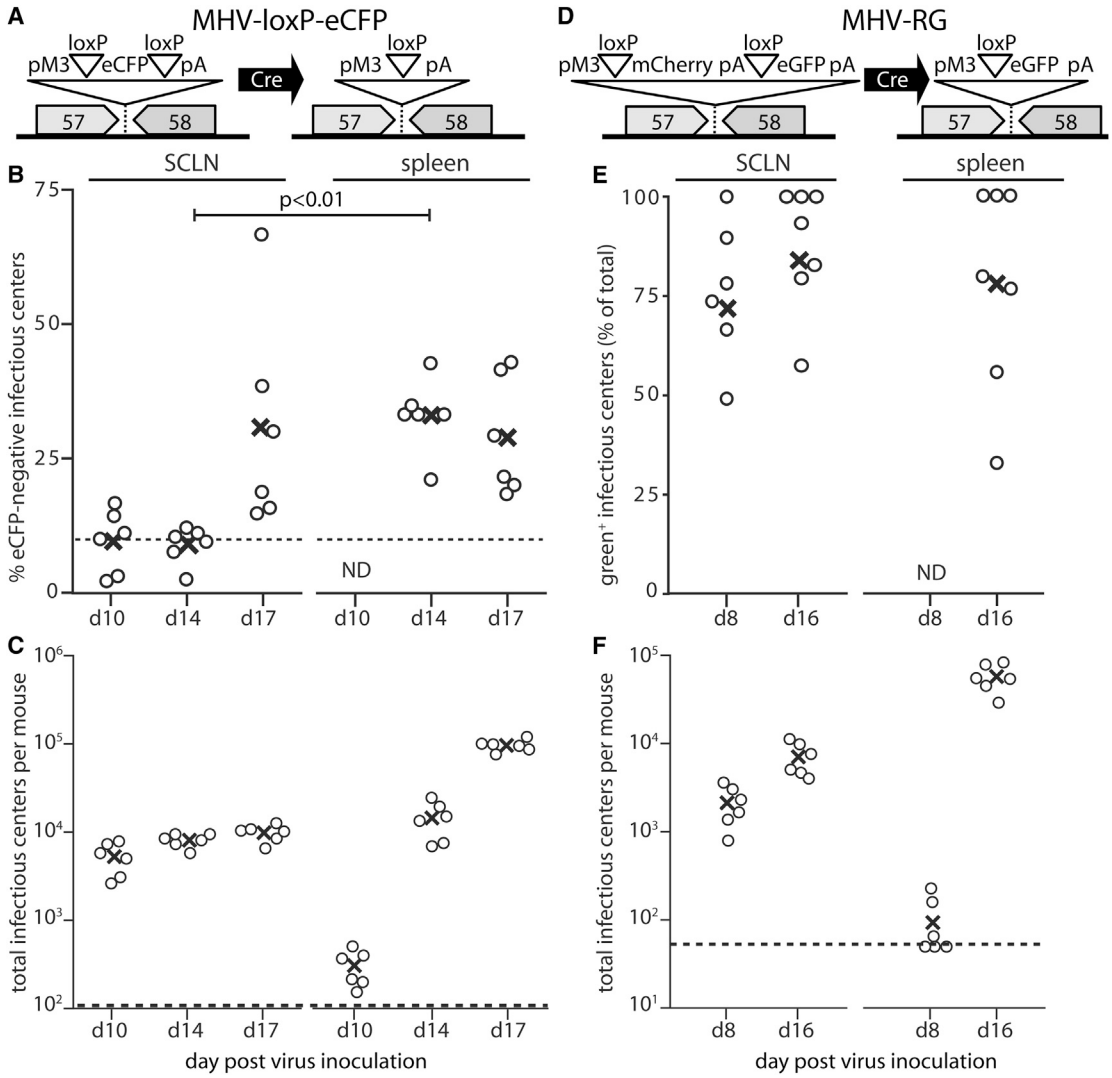

Figure 1. MuHV-4 Passes from LNs to Spleen via a LysM$^+$ Cell

(A) We infected LysM-cre mice i.n. with MHV-loxP-eCFP, which expresses eCFP from an intergenic viral M3 promoter. Cre recombinase removes the eCFP coding sequence via flanking loxP sites.

(B) Viruses recovered from LN and spleens by infectious center assay were scored as eCFP$^+$ or eCFP$^-$ under ultraviolet illumination. Recombination rate is the percentage of infectious centers that were eCFP negative. Circles show individual mice, crosses show means. ND = titers too low for reliable assay. Dashed lines show the detection limit for recombination (2 × eCFP$^-$ plaque frequency of nontransgenic controls).

(C) Total infectious center assay titers.

(D) We infected LysM-cre mice i.n. with MHV-RG, which expresses loxP-flanked mCherry upstream of eGFP. Cre converts it from mCherry$^+$eGFP$^-$ (red) to mCherry$^-$eGFP$^+$ (green).

(E) Viruses recovered from LN and spleens by infectious center assay were typed as red or green under ultraviolet illumination. Recombination rate (%) = 100 × green plaques/(green + red). No MHV-RG from nontransgenic controls was eGFP$^+$.

(F) Total infectious center assay titers. The dashed lines show lower detection limits.

lysM-cre DCs (Clausen et al., 1999) was evidently insufficient to recombine them en route to LN (Figure 1A). MHV-RG uses different loxP sites and is recombined more efficiently, fluorochrome expression switching from red to green (Frederico et al., 2012). It showed substantial switching in lysM-cre LN 8 days after i.n. infection (Figure 1B). Individual mice vary in lysM expression (Hume, 2011), and groups rarely exceeded a mean of 80% recombination (Figure 1B), so the day 8 recombination was already close to maximal, and neither spleens nor LN sampled at day 16 showed significantly more. Thus, en route to LN MuHV-4 infected lysM^{lo} cells that in lysM-cre mice recombined MHV-RG but not MHV-loxP-eCFP; then, en route to the spleen, it infected lysM^{hi} cells that also recombined MHV-loxP-eCFP.

In Situ Fluorochrome Switching Shows Macrophage Infection before B Cell Infection

I.n. MuHV-4 replicates in epithelial cells and LNs before reaching the spleen. The consequent achronicity of splenic infection

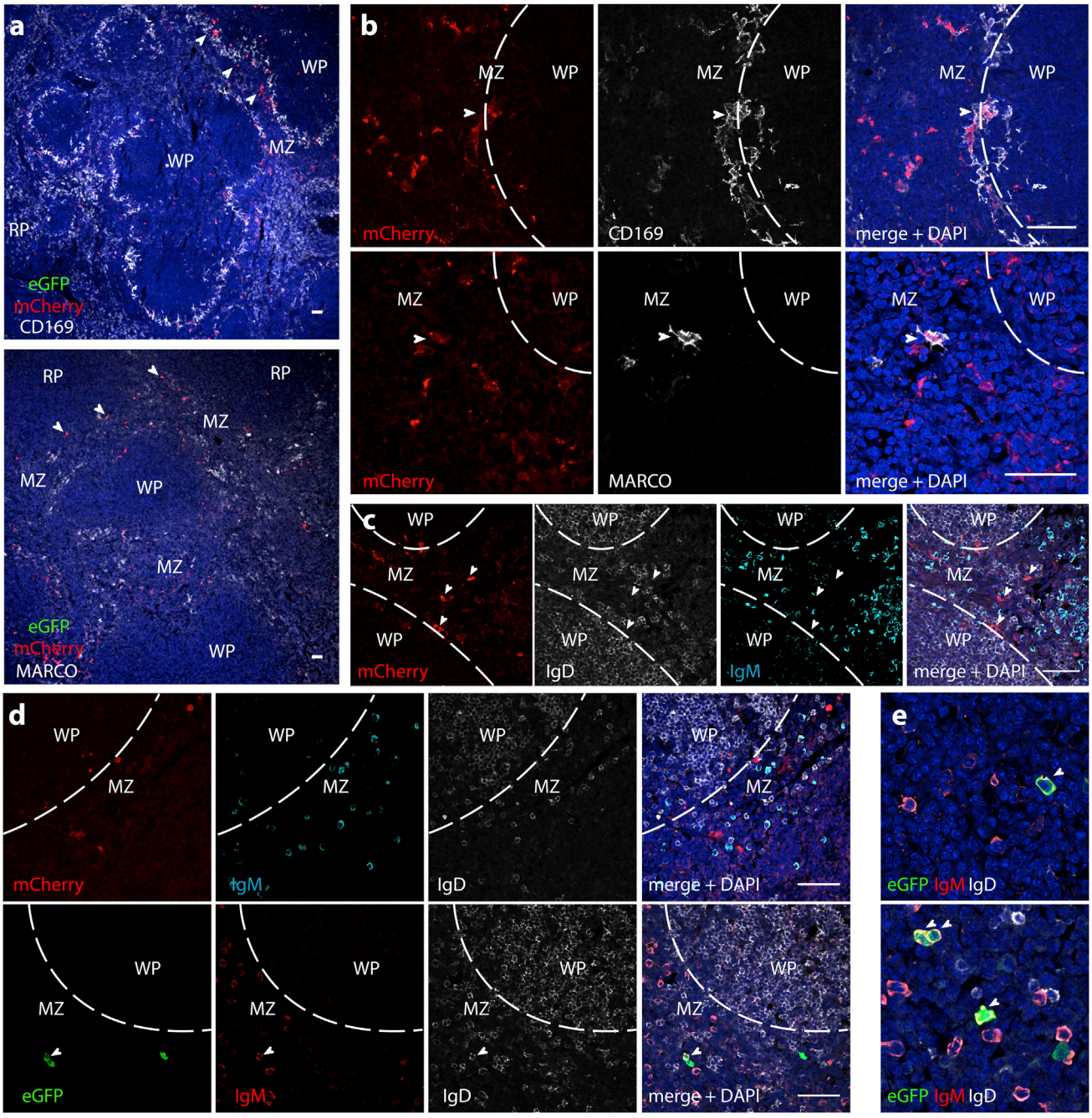

Figure 2. MuHV-4 Infects LysM$^+$ Splenic Macrophages before B Cells

(A) We infected LysM-cre mice i.p. with MHV-RG, and 4 days later stained spleen sections for mCherry (red) and CD169 or MARCO (white). Nuclei were stained with DAPI (blue). Arrows show red$^+$ cells in the MZ. Scale bar = 50 μm. Equivalent results were obtained in six mice.

(B) Higher-magnification MZ images show red$^+$CD169$^+$ and red$^+$MARCO$^+$ macrophages (arrows). Dashed lines mark MZ/WP borders.

(C) We infected mice as in (A) and 4 days later stained sections for mCherry (red), IgD (white), and IgM (cyan). Nuclei were stained with DAPI (blue). Arrows show mCherry$^+$ cells. None was IgM$^+$ or IgD$^+$. Equivalent results were obtained in six mice.

(D) We infected mice as in (A) and 8 days later stained spleen sections for mCherry (red), IgM (cyan), and IgD (white)—or for eGFP (green), IgM (red), and IgD (white). Again, no mCherry$^+$ cells were IgM$^+$ or IgD$^+$, but some eGFP$^+$ MZ cells were IgM$^+$IgD$^+$ (arrow). Equivalent results were obtained in 6 mice.

(E) Further examples of eGFP$^+$IgM$^+$ cells in the MZ (arrows). Figure 2, related to Figures S1 and S2.

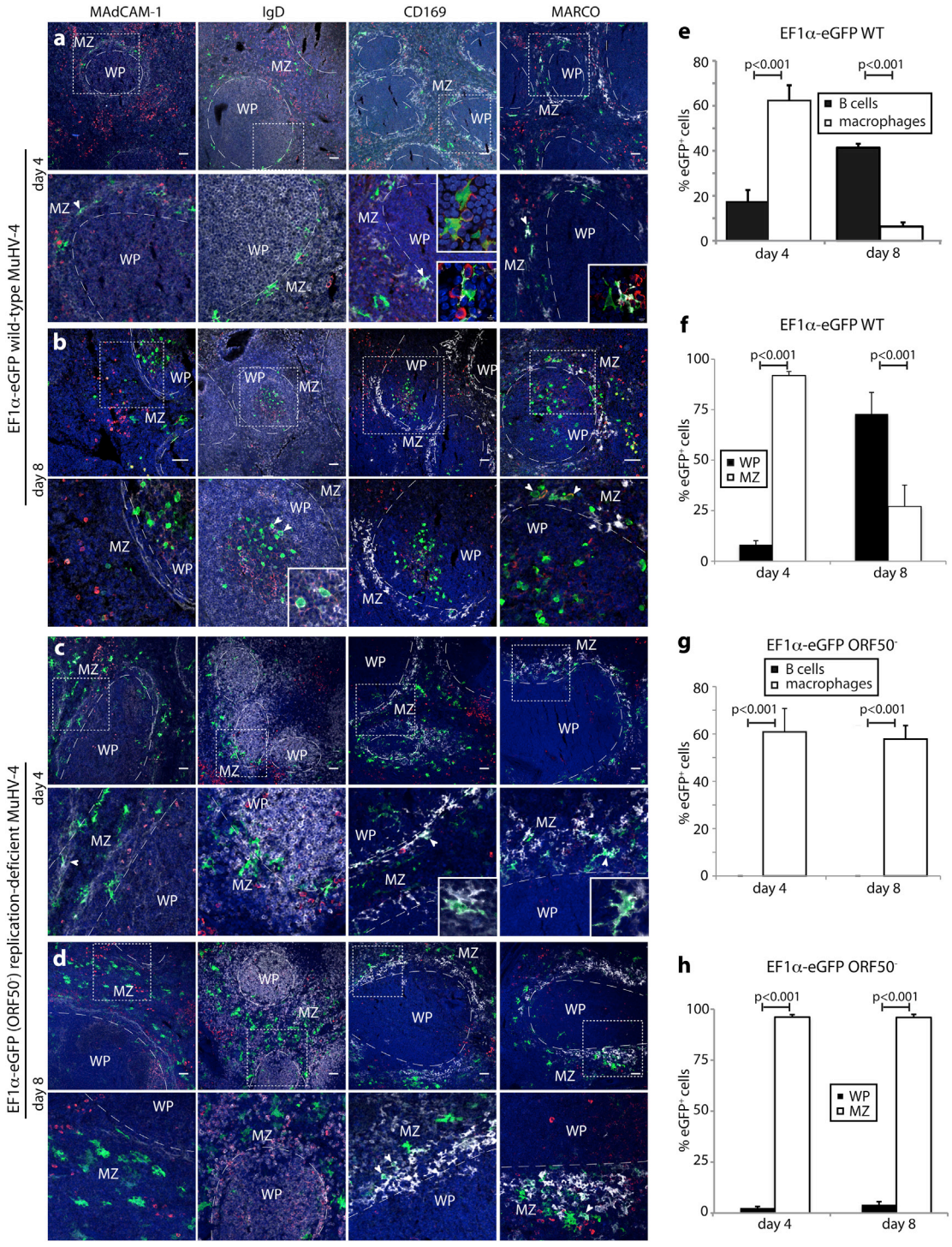

Figure 3. Only Replication-Competent MuHV-4 Reaches B Cells

(A–D) Examples of splenic infection by eGFP$^+$ MuHV-4. In (A), we infected C57BL/6J mice i.p. with EF1α-eGFP MuHV-4, and 4 days later stained spleen sections for eGFP (green) and IgM (red), plus either MARCO (MZ macrophages), CD169 (MZ metallophilic macrophages), IgD (follicular B cells), or MAdCAM-1 (endothelial cells) (white). Nuclei were stained with DAPI (blue). Dashed lines show MZ/WP boundaries. Scale bars = 50 μm. Upper panels show the overall staining distribution; lower panels show the boxed regions at higher magnification. Arrows show example eGFP$^+$ cells. The insets show examples of eGFP$^+$ macrophages contacting IgM$^+$ B cells in the MZ. In (B), mice infected as in (A) were analyzed after 8 days. Most eGFP$^+$ cells were now in the WP and IgD$^+$. Arrows in the IgD column show examples, as does the inset. Arrows in the MARCO column show IgM$^+$eGFP$^+$ MZ B cells. In (C), we infected C57BL/6J mice i.p. with replication-deficient (ORF50$^-$) EF1α-eGFP MuHV-4, and 4 days later we analyzed spleen sections as in (A) Arrows and insets show example eGFP$^+$ cells. None was IgM$^+$ or IgD$^+$. In (D), mice infected as in (C) were analyzed after 8 days. EGFP$^+$ cells remained in the MZ and were mostly CD169$^+$ or MARCO$^+$. None was IgM$^+$ or IgD$^+$.

(legend continued on next page)

makes it difficult to study just by this route. We therefore used also intraperitoneal (i.p.) virus inoculation. MHV-RG recovered from lysM-cre spleens 6 days later showed 61.5% ± 6.9% recombination (mean ± SD, 6 mice), so lysM$^+$ cells again provided an important gateway.

Blood enters the murine spleen via marginal sinuses, passing MZ metallophilic (CD169$^+$) and MZ (MARCO$^+$) macrophages to reach F4/80$^+$ red pulp (RP) macrophages (Figure S1). LysM-cre x Ai6 reporter mice, in which cre turns on ZsGreen production (Madisen et al., 2010), showed fluorescence in all these populations (Figure S2). To identify the cells responsible for MHV-RG recombination, we visualized it in situ. In this setting cre$^+$ cells infected by native MHV-RG can be mCherry$^+$, but downstream infected cells should be eGFP$^+$. Four days after i.p. infection, lysM-cre spleen sections showed mCherry$^+$ but not eGFP$^+$ cells (Figure 2A). Greater than 95% of the mCherry$^+$ cells were in the MZ: 45.7% ± 9.5% were CD169$^+$ and 31.7% ± 7.9% were MARCO$^+$ (mean ± SD, nine sections from three mice) (Figure 2B). No mCherry$^+$ cells were B cells (IgD$^+$ or IgM$^+$) (Figure 2C); by distribution and morphology, all were macrophages.

After 8 days (Figures 2D and 2E) 25.4% ± 3.9% of fluorescent cells in the MZ were eGFP$^+$ rather than mCherry$^+$. Again >85% of mCherry$^+$ cells were CD169$^+$ or MARCO$^+$ and none was IgD$^+$ or IgM$^+$ (Figure 2D, upper panels), but 25.2% ± 9.4% of eGFP$^+$ cells were IgM^{hi} (Figures 2D and 2E). Thus, i.p. virus reached splenic MZ macrophages without prior passage through a lysM$^+$ cell (at day 4 splenic macrophages were all mCherry$^+$eGFP$^-$), then gained access to IgM$^+$ MZ B cells (as these were not fluorescent until day 8 and were mCherry$^-$eGFP$^+$).

Viral eGFP Expression Shows MZ Infection before WP Infection

The M3 promoter driving MHV-RG fluorochrome expression is active mainly in lytic infection. To identify also latent infection, we tracked eGFP expression from a viral EF1α promoter (Frederico et al., 2012). Replication-competent or replication-deficient (ORF50$^-$) versions of this virus were given i.p. to mice, and spleen sections stained 4 and 8 days later for eGFP, macrophages (MARCO, CD169), B cells (IgD, IgM), and endothelial cells (MAdCAM-1) (Figure 3). Day 4 eGFP expression was largely confined to the MZ, and most eGFP$^+$ cells were CD169$^+$ or MARCO$^+$ (Figures 3A and 3E). Close apposition was evident between eGFP$^+$ macrophages and IgM^{hi} B cells (Figure 3A, insets), consistent with infection transfer, and by day 8 (Figures 3B and 3F) significantly more eGFP$^+$ cells were B cells and inside WP follicles ($p < 0.001$). Some MAdCAM-1$^+$ endothelial cells were also eGFP$^+$ (Figure 3A). However, there were 30–40 eGFP$^+$ macrophages and only 0–1 eGFP$^+$MAdCAM-1$^+$ cells per follicle, so infection moved mostly from macrophages to B cells. Comparing fluorochrome expression from M3 (Figure 2) and EF1α promoters (Figure 3) suggested that a substantial fraction of MZ infection was lytic, whereas most WP infection was latent (or abortive).

Replication-Deficient MuHV-4 Is Arrested in MZ Macrophages

ORF50$^-$ MuHV-4 fails to replicate without complementation and so marks only the first infected cells. Four days after i.p. EF1α-eGFP$^+$ORF50$^-$ MuHV-4, >95% of splenic eGFP$^+$ cells were CD169$^+$ or MARCO$^+$ macrophages and none was IgM$^+$ or IgD$^+$ (Figures 3C and 3G). Some MAdCAM-1$^+$ endothelial cells were eGFP$^+$ but, again, they were sparse (0–1 per follicle). Day 8, infection remained overwhelmingly in MZ macrophages (Figures 3D and 3H; $p < 0.001$). Thus, i.p. infection directly reached MZ macrophages and not B cells.

Functional Evidence that Splenic Macrophage Infection Precedes Splenic B Cell Infection

To establish functionally that macrophage infection precedes B cell infection, we gave MHV-RG i.p. to lysM-cre or CD19-cre mice, recovered viruses by infectious center assay, and typed them for recombination (Figure 4A). At day 1, CD19-cre spleens yielded no eGFP$^+$ virus, while that from lysM-cre spleens was >25% eGFP$^+$. Virus from lysM-cre peritoneal washes also switched, but this did not account for the splenic switching, as i.p. virus reached splenic macrophages directly (Figure 3) without prior recombination (Figure 2). CD19-cre spleens yielded >50% eGFP$^+$ virus at day 8, so these mice efficiently recombined MHV-RG once B cells were infected. Therefore, splenic B cells were not infected until after splenic macrophages.

MZ B Cells Take MuHV-4 to WP Follicles

After passing from MZ macrophages to MZ B cells, EF1α-eGFP MuHV-4 entered the WP (Figure 3B). A cellular vehicle for this movement seemed likely, as cell-free virions would follow MZ blood flow to the RP (Figure S1). Macrophage migration seemed unlikely, as eGFP$^+$CD169$^+$ and eGFP$^+$MARCO$^+$ cells remained in the MZ and eGFP$^+$F4/80$^+$ macrophages remained in the RP (Figure 4B). However, CD1d$^+$eGFP$^+$ cells were abundant in the MZ at day 4 (Figures 4C and 4D), and in the WP at day 8, whereas no WP cells were CD1d$^+$ at day 4—or in naive mice (data not shown). These were therefore a plausible candidate for virus transfer. MZ B cells express CD1d (Makowska et al., 1999), can transport antigens to the WP (Lopes-Carvalho and Kearney, 2004; Cerutti et al., 2013), and communicated with infected MZ macrophages (Figure 3). The CD1d$^+$eGFP$^+$ cells in the MZ at day 4 were IgM^{hi} (Figure 4D). Those in the WP at day 8 stained poorly for IgM, suggesting that they may have differentiated into plasma cells, a key γHV reactivation trigger (Laichalk and Thorley-Lawson, 2005; Liang et al., 2009).

We sought functional evidence for MZ B cell involvement in infection spread by driving them prematurely into the WP with the sphingosine-1-phosphate receptor agonist FTY720 (Cinamon et al., 2004). Mice treated with drug or not were given i.p. EF1α-eGFP MuHV-4 (Figures 4E and 4F). At day 4, drug-treated and untreated mice showed similar numbers of eGFP$^+$ MZ macrophages, but at day 8 drug-treated mice had

(E–H) Quantitation across multiple sections. In (E) and (F), mice were infected and analyzed as in (A) and (B). EGFP$^+$ cells were counted for at least five follicles/MZs for each of five mice. Bars show mean ± SEM. In (E), eGFP$^+$ cells were scored as MZ macrophages (CD169$^+$ or MARCO$^+$) or B cells (IgM$^+$ or IgD$^+$). In (F), eGFP$^+$ cells were scored by their position relative to the MAdCAM-1$^+$ endothelial cells separating the WP and MZ. In (G) and (H), mice were infected and analyzed as in (C) and (D) and scored as in (E) and (F).

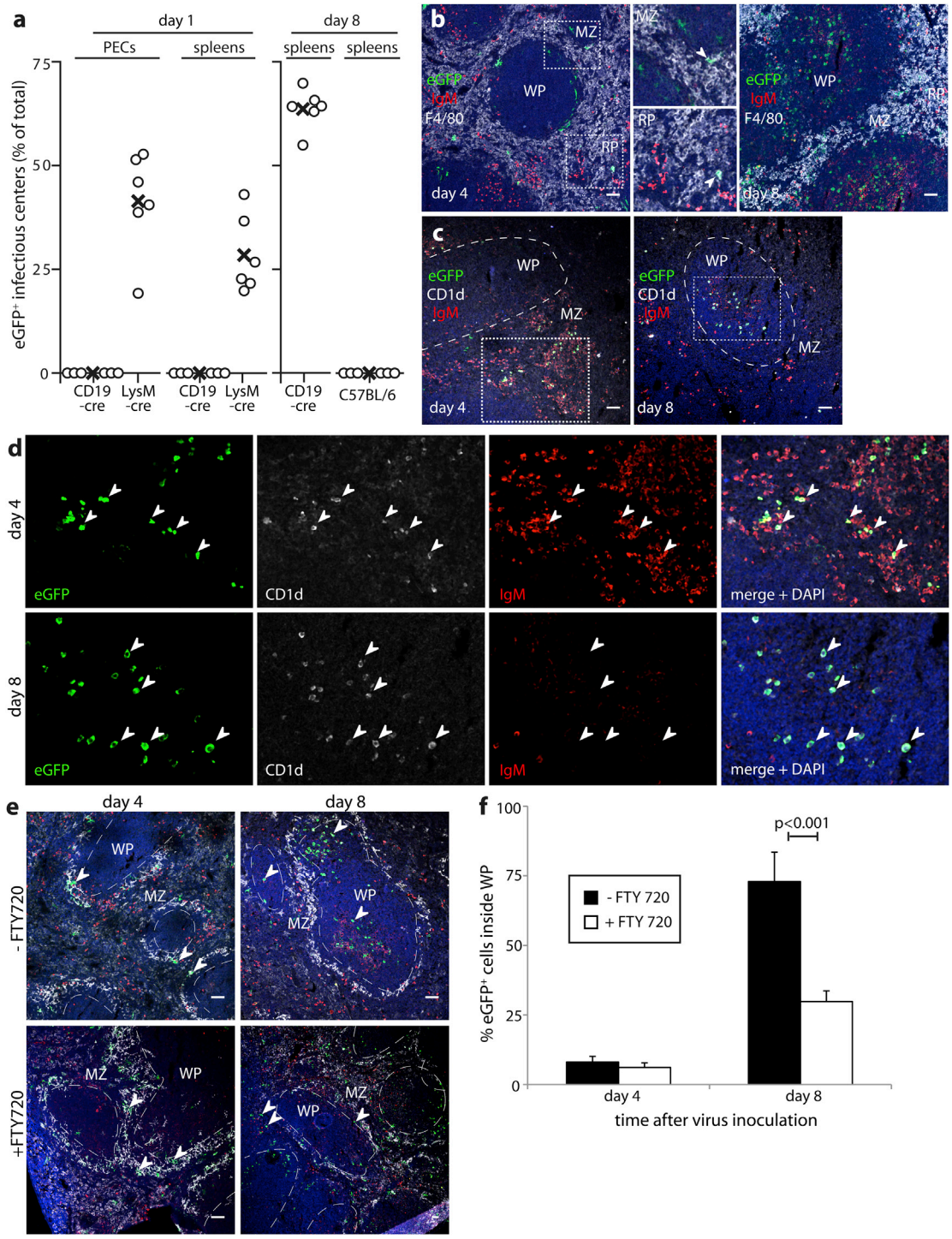

Figure 4. CD19$^+$ B Cells Are Infected after LysM$^+$ Myeloid Cells and Then Relocate to the WP

(A) We infected LysM-cre, CD19-cre, and C57BL/6J mice i.p. with MuHV-RG. Viruses were recovered from spleens and peritoneal washes by infectious center assay 1 or 8 days later and scored as red (native) or green (recombined). Recombination rate = 100 × green / (green + red). Circles show individual mice, crosses show means. At day 1, recombined viruses were recovered from lysM-cre but not CD19-cre mice. At day 8 recombined viruses were recovered from CD19-cre but not C57BL/6J mice.

(B) We infected C57BL/6J mice i.p. with EF1α-eGFP MuHV-4, and 4 and 8 days later stained spleen sections for eGFP (green), IgM (red), and macrophages (F4/80, white). Nuclei were stained with DAPI (blue). The middle panels show the day 4 MZ and RP boxed regions at higher magnification. Arrows show eGFP$^+$F4/80$^+$ macrophages. By day 8, eGFP was mainly in the WP; F4/80 staining remained in the MZ / RP. Scale bars = 50 μm. Equivalent results were obtained in three mice.

(legend continued on next page)

significantly fewer eGFP$^+$ WP cells, consistent with an important MZ B cell role in MZ to WP MuHV-4 transfer.

Virus Transfer via Follicular DCs

MuHV-4 persists in GC-derived memory B cells (Willer and Speck, 2003), and at day 8 of i.p. infection eGFP$^+$PNA$^+$ cells were evident in splenic WP follicles (Figures 5A and 5B). MZ B cells can enter GCs (Cerutti et al., 2013). However, this is more commonly a function of follicular B cells, and as these also harbor MuHV-4 genomes (Marques et al., 2003), they seemed a more likely route to GC exploitation. MZ and follicular B cells are not known to interact, but both interact with follicular DCs. After EF1α-eGFP MuHV-4 inoculation, CR1/2$^+$ follicular DCs remained eGFP$^-$ (Figures 5C–5E). However, they were closely associated with eGFP$^+$ WP B cells (Figure 5D), and at day 4, virion antigens were evident on CR1/2$^+$ DC processes (Figure 5E). None was seen on the follicular DCs of mice infected with replication-deficient (ORF50$^-$) MuHV-4, so they were a product of lytic spread. Thus, MuHV-4 produced by MZ B cells appeared to reach GC B cells via follicular DCs. The uniform small size of viral antigen$^+$ particles on DCs (<1 μm diameter) suggested that many of these were virions rather than infected cell debris.

Intranasal Virus Infects the Spleen Similarly to Intraperitoneal Virus

Nine days after i.n. EF1α-eGFP MuHV-4, when infection first reaches the spleen, eGFP$^+$CD19$^+$ splenic B cells showed higher CD35 expression and lower CD23 expression than eGFP$^-$CD19$^+$ cells, consistent with MZ B cells (CD19$^+$CD23^{lo}CD35^{hi}) being an early target (Figure 5F). Spleen sections showed eGFP$^+$CD169$^+$ MZ macrophages (Figure 5G), IgM^{hi}eGFP$^+$ MZ B cells, B220$^+$eGFP$^+$ WP B cells (Figure 5H), and the intermediate step of eGFP$^+$IgM^{hi} WP B cells (Figure 5I). Thus, i.p. and i.n. infections showed the same component steps of splenic colonization. Because i.n. virus must traverse the olfactory epithelium and LNs, splenic infection was less synchronous and its different stages consequently less distinct—when eGFP$^+$ cells were abundant in most MZs, some follicles already showed spread to the WP. Nonetheless, MZ involvement was clear.

A Lack of MZ B Cells Impairs Splenic Infection by Intranasal and Intraperitoneal MuHV-4

We next sought functional evidence for MZ involvement in splenic colonization by i.n. MuHV-4. As FTY720 disrupts both spleen and LN lymphocyte traffic (Cinamon et al., 2004), we instead used CD19$^{-/-}$ mice as a MZ B cell-deficient mutant (Martin and Kearney, 2000) that otherwise makes normal acute responses to viral infection (Fehr et al., 1998). Nose and lung infections were comparable between CD19$^{-/-}$ and CD19$^{+/+}$ mice (Figure 6A). However, CD19$^{-/-}$ lymphoid infections were significantly reduced (Figure 6B), as were CD19$^{-/-}$ viral genome loads (Figure 6C). The reduction in infectious centers titers was significantly greater for spleens ($p < 0.01$), and immunostaining for viral eGFP at day 10 (Figure 6D) showed B cell infection in CD19$^{+/+}$ and CD19$^{-/-}$ LNs and CD19$^{+/+}$ but not CD19$^{-/-}$ spleens.

CD19 deficiency also impaired spleen infection (but not peritoneal exudate cell infection) by i.p. virus, as measured by infectious center assay (Figure 6E), viral DNA load (Figure 6F), and immunostaining (Figure 6G). Thus, CD19$^{-/-}$ mice showed a general defect in B cell infection, and a particular defect in splenic infection, consistent with an important role here for MZ B cells.

B Cell Colonization Depends on Virus-Driven Intercellular Spread

The close parallels between MuHV-4 spread and host immune pathways suggested that the virus might be a merely passive passenger. To test this, we analyzed MuHV-4 lacking ORF27, which encodes a glycoprotein necessary for efficient intercellular spread (May et al., 2005) and conserved in KSHV (ORF27) and EBV (BDLF2). After i.p. inoculation, ORF27$^-$ infectious centers were similar to ORF27$^+$ in peritoneal exudate cells but reduced in spleens (Figure 7A). Splenic viral genome loads were also reduced (Figure 7B). A similar phenotype was observed with an independent ORF27 mutant, while a revertant virus replicated like wild-type (Figure 7C). We determined the long-term consequences of ORF27 deficiency by giving mice 3:1 mixtures of marker-distinguished ORF27$^-$ and ORF27$^+$ viruses i.p., then marker-typing splenic virus 1 month later (Figure 7D). Recovered splenic virus was consistently enriched for ORF27$^+$. Thus, a lack of ORF27 impaired both acute and long-term splenic infection.

Splenic sections (Figures 7E and 7F) showed that both ORF27$^-$eGFP$^+$ and ORF27$^+$eGFP$^+$ viruses colonized MZ macrophages by day 4, but only ORF27$^+$ efficiently formed eGFP$^+$ WP follicles by day 8: ORF27$^-$ virus remained largely in the MZ. Thus, a lack of ORF27 did not impair virus entry into macrophages, consistent with normal peritoneal exudate titers (Figure 7A), but impaired subsequent spread to WP B cells. Therefore, MuHV-4 was not just a passive participant in intercellular exchanges but actively promoted them to enhance host colonization.

DISCUSSION

Lymphocytes must confront invading pathogens, but a capacity for proliferation and dissemination makes their own infection a potential hazard. Myeloid cells consequently play an important,

(C) We infected mice as in (B) and stained spleens 4 or 8 days later for eGFP (green), CD1d (white), and IgM (red). Nuclei were stained with DAPI (blue). Again, day 4 eGFP was in the MZ and day 8 eGFP in the WP. Equivalent results were obtained in six mice.
(D) The boxed regions of (C) at higher magnification with separate channels. Arrows show IgM$^+$CD1d$^+$eGFP$^+$ cells in the MZ at day 4 and eGFP$^+$CD1d$^+$ cells in the WP at day 8.
(E) Mice treated or not with the sphingosine-1-phosphate receptor agonist FTY720 to dislocate MZ B cells prematurely to the WP were infected as in (B). Spleen sections were stained for eGFP (green), IgM (red), and CD169 (white). Nuclei were stained with DAPI (blue). At day 4, both treated and untreated mice had eGFP$^+$ cells in the MZ. Arrows show eGFP$^+$CD169$^+$ MZ macrophages. At day 8 most eGFP$^+$ cells of untreated mice were in the WP, while those of treated mice remained in the MZ (arrows).
(F) Mean ± SEM counts per section, scoring eGFP$^+$ cells as inside or outside the WP for three to four sections from each of three mice per group.

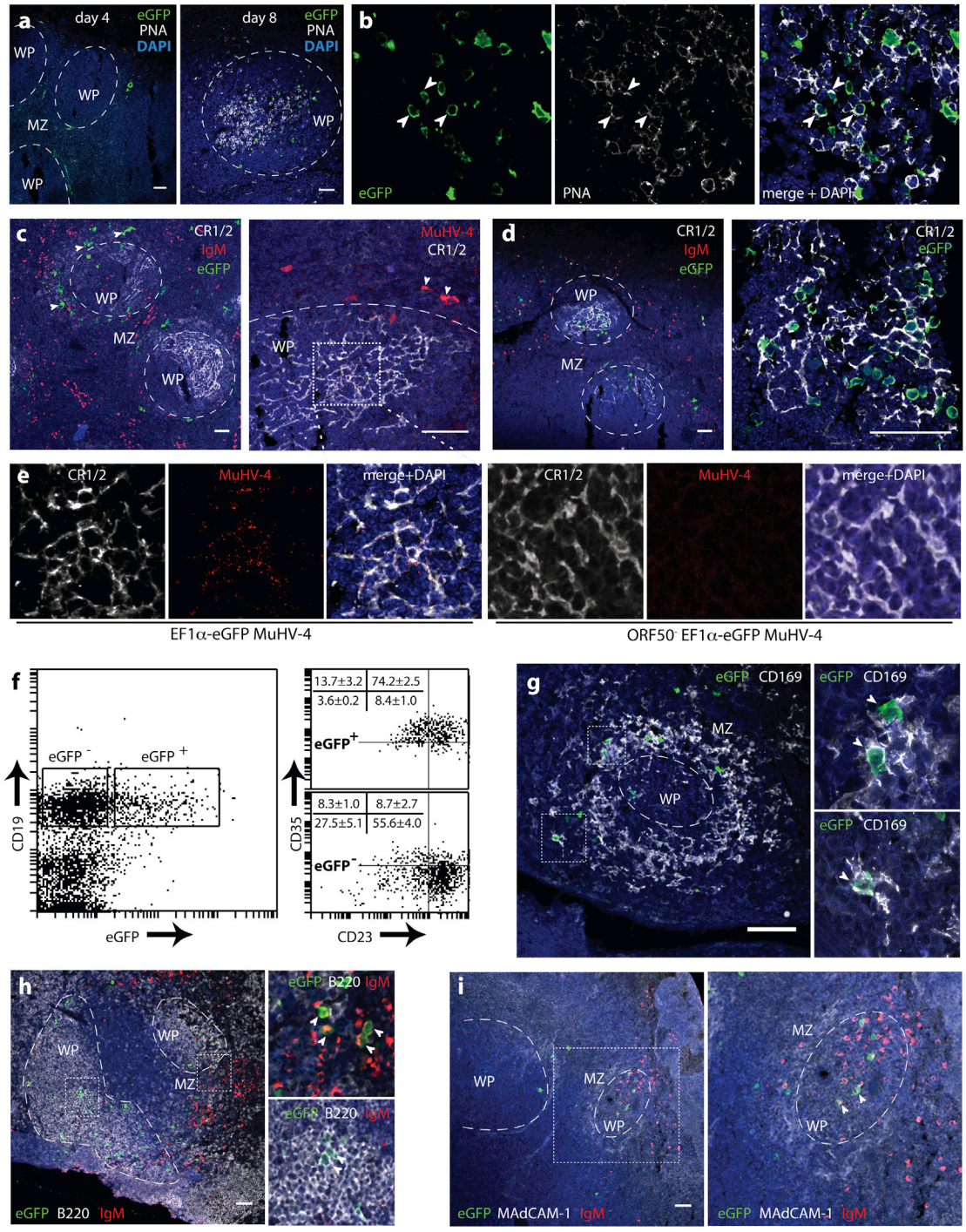

Figure 5. Virus Transfer to Follicular B Cells via Follicular DCs and Similar Infection by Intranasal MuHV-4

(A) We infected C57BL/6J mice i.p. with EF1α-eGFP MuHV-4 and 4 or 8 days later stained spleen sections for eGFP (green) and with PNA (white). Nuclei were stained with DAPI (blue). Dashed lines show WP/MZ boundaries. At day 4, most eGFP$^+$ cells were in the MZ, and few WP cells were PNA$^+$; at day 8, most eGFP$^+$ cells were in the WP and many WP cells were PNA$^+$. Scale bars = 50 μm. Equivalent results were obtained in three mice.

(B) A higher magnification view of the WP at day 8, with eGFP$^+$PNA$^+$ cells (arrows).

(C and D) We then infected mice as in (A), and 4 or 8 days later, stained spleen sections (C and D) for complement receptors 1/2 (CR1/2, white), which are highly expressed on follicular DCs, and for either IgM (red) plus eGFP (green) or for viral antigens (MuHV-4, red). Nuclei were stained with DAPI (blue). Scale bars = 50 μm. Dashed lines outline WP follicles. Equivalent results were obtained in three mice. Arrows in (C) show eGFP$^+$ and MuHV-4$^+$ MZ cells with morphologies typical of macrophages. (D) shows eGFP$^+$ B cells closely associated with CR1/2^{hi} eGFP$^-$ follicular DCs. (E) The left-hand panels show the boxed region of (C) at higher magnification, with MuHV-4 antigens on CR1/2$^+$ DC processes. The right-hand panels show no viral antigens on the DCs of a mouse infected with replication-deficient MuHV-4 (ORF50$^-$).

(legend continued on next page)

front-line role in pathogen processing and presentation. γHVs colonize lymphocytes nonetheless. How has been unclear. MuHV-4 spread by serial virus exchange along normal immune communications. An important implication is that appropriate immunity to lytic antigens could restrict γHV dissemination.

I.n. MuHV-4 reaches the SCLN via a $CD11c^+$ cell (Gaspar et al., 2011). Essentially, all the virus recoverable from SCLN has also passed through a B cell (Frederico et al., 2012) and i.n. virus does not reach the spleens of B cell-deficient mice (Usherwood et al., 1996). Therefore, SCLN B cell infection is the next step. The next anatomical target is the spleen, where B cell infection again predominates. However, infected splenic B cells seem not to descend directly from SCLN B cells, and MuHV-4 reached splenic follicular B cells only via MZ macrophages, MZ B cells, and follicular DCs. This would explain why γHV infectious mononucleosis elicits strong T cell responses to lytic antigens (Callan et al., 1996; Stevenson et al., 1999). Spread via specialized macrophages is consistent with their emerging role in antigen presentation to B cells (Junt et al., 2007; Carrasco and Batista, 2007; Phan et al., 2009).

To infect MZ macrophages, MuHV-4 must reactivate from SCLN B cells. Reactivation is associated with plasma cell differentiation. Potentially, this could occur in the MZ, but while MZ B cells differentiate here, it is not classically a differentiation site for LN-derived memory B cells. Also, a freely circulating B cell would traverse the spleen >300 times a day (Chen and Kaufman, 1996), so in the long term, a tendency to reactivate here would severely deplete the latent pool. LN medullary cords are a prominent site of plasma cell differentiation (Fooksman et al., 2010), and acute viral lytic gene expression is evident in the SCLN (Figure S3). Thus, we hypothesize that MuHV-4 reaches the spleen after being shed into the efferent lymph by reactivating SCLN B cells. We detect cell-free MuHV-4 DNA in only 40%–50% of acute serum samples (data not shown), but at this time virus loads are still low—they are amplified primarily in the spleen—and released virions may have only a short half-life in the blood, making detection difficult. Acute viremia consistent with vascular spread is well known for EBV (Gan et al., 1994).

In passing from MZ macrophages to MZ B cells, follicular DCs, and then GC B cells, MuHV-4 followed normal immune communication pathways. Direct spread from MZ macrophages to follicular B cells (Arnon et al., 2013) is also possible, but MZ B cells seemed to provide the main route. MuHV-4 amplified these exchanges with ORF27—which promotes intercellular virus spread via fine, virus-laden actin protrusions (Gill et al., 2008). Diverse actin-based intercellular connections have been identified for viruses spreading in vitro (Xu et al., 2009), and MuHV-4 also induces large-scale cytoskeletal reorganization in infected myeloid cells (Smith et al., 2007) consistent with the envelopment of MZ B cells by infected $CD169^+$ MZ macrophages. (ORF27-induced protrusions are much finer and visible only at higher magnification.)

Follicular DCs appeared to transfer virus without becoming infected, analogous to their presentation of immune complexes to GC B cells. Similar transfers have been described in vitro (Piguet and Steinman, 2007). Follicular DCs— like in vitro activated DCs (Smith et al., 2007)—may resist infection because they poorly transport antigens to late endosomes (Chen et al., 1978), the site of MuHV-4 membrane fusion (Gillet et al., 2008). Transferred virions could still acquire B cell tropism (Frederico et al., 2012), as the key glycoprotein conformation changes occur in early endosomes (Glauser et al., 2012).

EBV drives splenomegaly and exploits GCs, and KSHV infects GC macrophages (Valmary et al., 2005). However, the precise paths these viruses follow must remain speculative: human spleens also capture and respond to blood-borne antigens (Weill et al., 2009), but their marginal sinuses and associated macrophages occupy a peri-follicular zone rather than the MZ (Steiniger et al., 1997). EBV lytic spread has been inferred from histological analysis of infected tonsils (Kurth et al., 2000), but clinical presentation occurs relatively late in infection, and conclusions must be drawn from single time points. Our data showed events changing dramatically with time; serial tracking, virus marking, and a replication-deficient mutant were all necessary to understand a highly complex process.

In vitro EBV analysis has concentrated on cell-free virions (Borza and Hutt-Fletcher, 2002); in vivo infection may pass more from cell to cell. This is hard for antibody to block, possibly explaining the failure of gp350-specific antibodies to reduce EBV infection rates (Sokal et al., 2007). Targeting the cells that collect virions for transfer to B cells could work better. For MuHV-4 this was myeloid cells. Myeloid infection has been reported also for EBV (Savard et al., 2000; Guerreiro-Cacais et al., 2004; Walling et al., 2007). MuHV-4 elicits antibody responses that neutralize myeloid infection poorly and instead enhance it via IgG Fc receptor binding (Rosa et al., 2007; Gillet et al., 2007a). However vaccine-induced antibodies to gH/gL can block infection (Gillet et al., 2007b). Thus, understanding MuHV-4 dissemination suggests a possible approach to γHV infection control.

EXPERIMENTAL PROCEDURES

Mice

BALB/c, C57BL/6J (Harlan UK), LysM-cre (Jackson Laboratories) (Clausen et al., 1999), and CD19-cre mice (kindly provided by M. Turner, Babraham

(F) We infected C57BL/6J mice i.n. with EF1α-eGFP MuHV-4 and 9 days later analyzed $eGFP^-$ and $eGFP^+$ B cells ($CD19^+$) for CD23 and CD35 expression by flow cytometry. The numbers show mean ± SD percentages of gated cells in each quadrant for six mice in two experiments. $EGFP^+$ rates were significantly lower in $CD35^{lo}CD23^{hi}$ (follicular) B cells ($p < 0.0001$) and significantly higher in $CD35^{hi}CD23^{lo}$ (MZ) B cells ($p < 0.003$).

(G) We infected mice as in (F) and 9 days later stained spleen sections for eGFP (green) and CD169 (white). Nuclei were stained with DAPI (blue). The left-hand image shows the overall distribution of eGFP staining (scale bar = 50 μm). The right-hand panels show the boxed regions at higher magnification, with examples of $eGFP^+CD169^+$ MZ macrophages. Equivalent results were obtained in six mice.

(H) We infected mice as in (F) and 9 days later stained spleen sections for eGFP (green), B220 (white), and IgM (red). Nuclei were stained with DAPI (blue). The left-hand image shows the overall distribution of staining (scale bar = 50 μm); the right-hand panels show the boxed regions at higher magnification. Arrows show $eGFP^+IgM^+$ MZ B cells and $eGFP^+B220^+$ follicular B cells. Equivalent results were obtained in six mice.

(I) We infected mice as in (F) and 9 days later stained spleen sections for eGFP (green), MAdCAM-1 (white), and IgM (red). Nuclei were stained with DAPI (blue). The left-hand panel shows the overall distribution of eGFP staining (scale bar = 50 μm); the right-hand panel shows the boxed region at higher magnification. Arrows show $eGFP^+IgM^{hi}$ cells in the WP. Equivalent results were obtained in 6 mice. Figure 5, related to Figure S3.

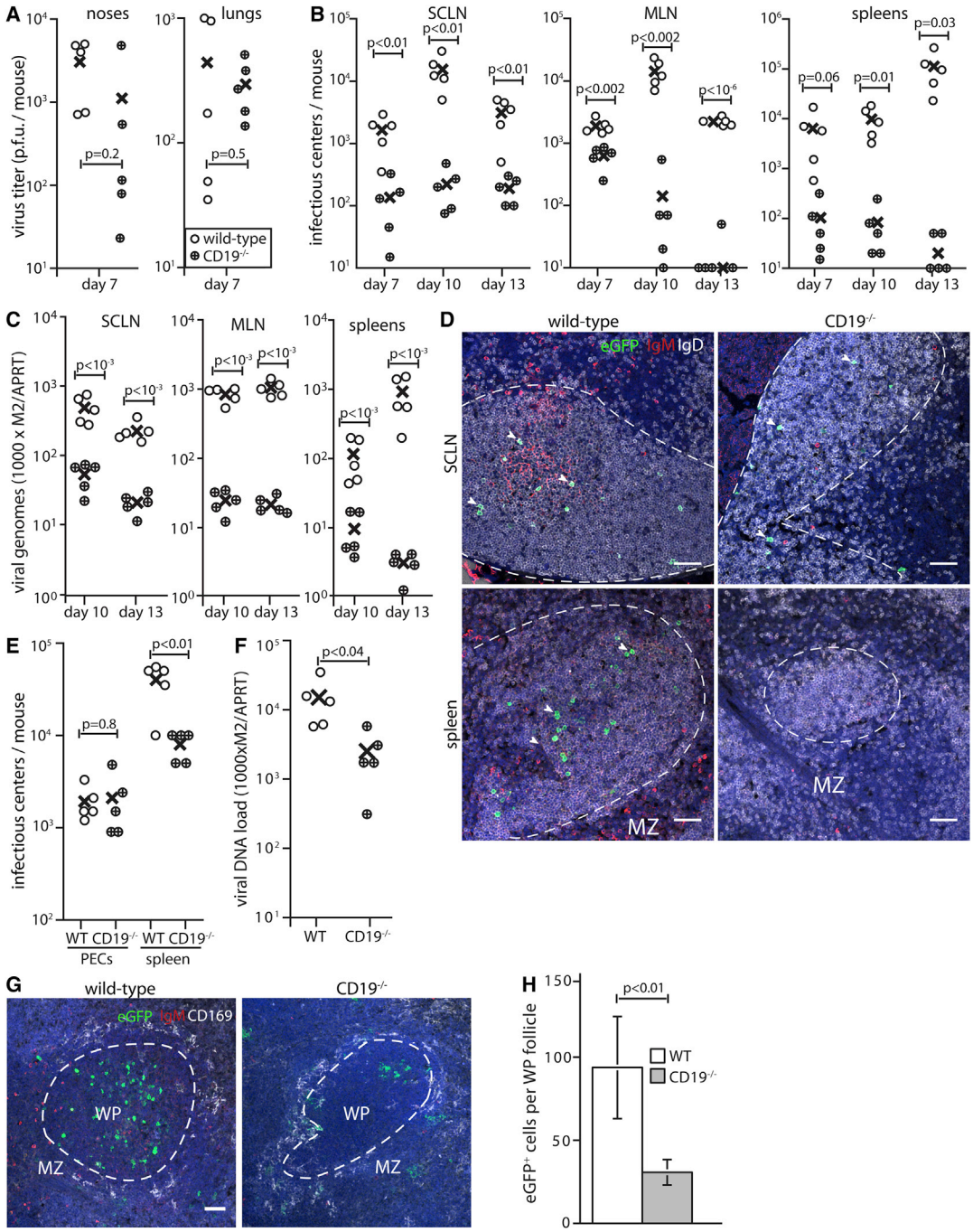

Figure 6. CD19 Deficiency Severely Compromises MuHV-4 Host Colonization

(A) We infected wild-type or CD19$^{-/-}$ mice i.n. with MuHV-4 and 7 days later measured infectious virus in noses and lungs by plaque assay. Circles show individual mice; crosses show means. Horizontal bars show statistical comparisons.

(B) We infected mice as in (A) and measured viral loads in superficial cervical lymph nodes (SCLN), mediastinal lymph nodes (MLN), and spleens by infectious center assay 7, 10, and 13 days later.

(C) Lymphoid tissue of the day 10 and 13 mice in (B) was assayed for viral genomes (M2) by Q-PCR. Results are normalized by cellular DNA copy numbers (APRT).

(D) We infected wild-type and CD19$^{-/-}$ mice i.n. with EF1α-eGFP MuHV-4 and stained LN and spleens 10 days later for eGFP (green), IgM (red), and IgD (white). Nuclei were stained with DAPI (blue). Dashed lines outline B cell follicles. Scale bars = 50 μm. Arrows show eGFP^{+} cells, which were absent from CD19$^{-/-}$ spleens.

(E) We infected wild-type or CD19$^{-/-}$ mice i.p. with EF1α-eGFP MuHV4 and recovered viruses 8 days later by infectious center assay.

(F) We infected mice as in (E) and measured splenic viral genome loads (M2) by Q-PCR, normalized by cellular DNA copy numbers (APRT).

(G) We infected mice as in (E) and stained spleen sections 8 days later for eGFP (green), IgM (red), and CD169 (white). Nuclei were stained with DAPI (blue). Dashed lines outline WP follicles. Scale bar = 50 μm.

(H) We counted eGFP^{+} cells on spleen sections and scored them as within or the WP or not (mean ± SEM for five mice, counting 15 follicles each).

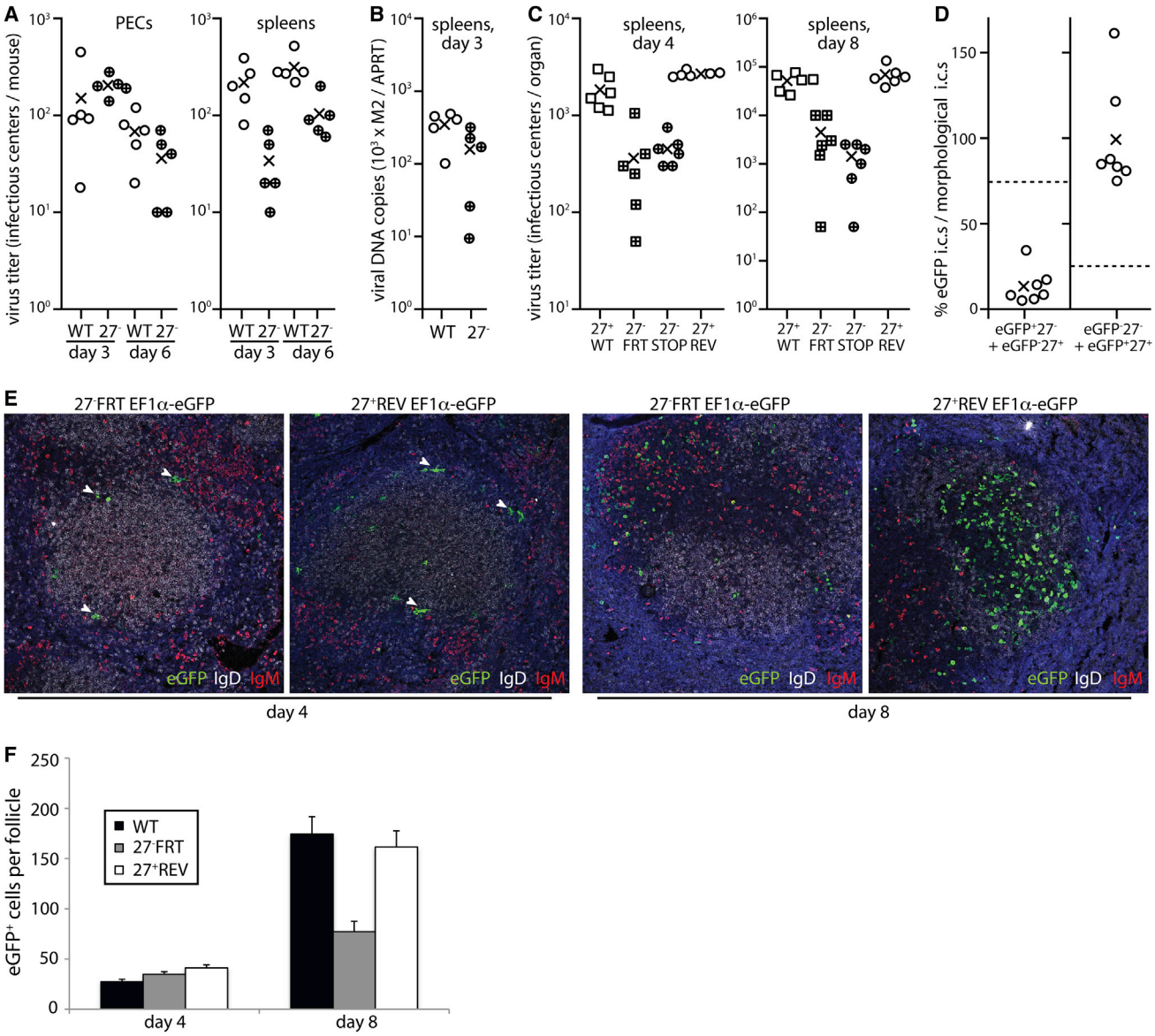

Figure 7. Efficient GC Colonization Requires the MuHV-4 ORF27

(A) We infected C57BL/6J mice i.p. with ORF27$^+$ (WT) or ORF27$^-$ FRT (27$^-$) EF1α-eGFP$^+$ MuHV-4, then titered peritoneal exudate cell (PECs) and spleens for virus by infectious center assay 3 and 6 days later. Circles show individual mice; crosses show means. WT and ORF27$^-$ PEC titers were not significantly different ($p > 0.15$), but ORF27$^-$ spleen titers were significantly reduced ($p < 0.01$).

(B) Splenic viral genome loads measured by Q-PCR also showed a significant, ORF27-dependent reduction ($p < 0.03$).

(C) We infected C57BL/6J mice i.p. with ORF27$^+$ (WT or revertant of 27$^-$FRT = REV) or ORF27$^-$ (27$^-$FRT or 27$^-$STOP) viruses—this time without EF1α-eGFP—and measured splenic viral loads by infectious center assay 4 and 8 days later. ORF27$^-$ viruses showed significantly lower titers at both day 4 ($p < 0.002$) and day 8 ($p < 0.0002$).

(D) We mixed 27$^-$FRT EF1α-eGFP$^+$ MuHV-4 with the unlabelled revertant (ORF27$^+$) (3:1 ratio, left-hand panel), or 27$^-$STOP MuHV-4 with the EF1α-eGFP$^+$ WT (3:1 ratio, right-hand panel), then infected mice i.p. (total 10^5 p.f.u.), and 1 month later typed the viruses recovered by infectious center assay as eGFP$^+$ or eGFP$^-$. Circles show the percentage of eGFP of virus recovered from each mouse. Crosses show means. Because eGFP fluorescence makes plaques more obvious, eGFP$^+$ plaque counts could exceed morphological plaque counts; any counting bias was controlled by having the eGFP tag on ORF27$^-$ virus in one mixture and ORF27$^+$ in the other. Dashed lines show percentage of eGFP of the input virus. For each infection the recovered ORF27$^-$ proportion was significantly less than the input ($p < 0.001$).

(E) We infected C57BL/6J mice i.p. with EF1α-eGFP$^+$ ORF27$^-$FRT MuHV-4 or its ORF27$^+$ revertant (REV). Four and eight days later we stained spleen sections for eGFP (green), IgD (white), and IgM (red). Nuclei were stained with DAPI (blue). Day 4 arrows show infected MZ macrophages (eGFP$^+$IgD$^-$IgM$^-$). Day 8 shows abundant ORF27$^+$eGFP$^+$ infection in the splenic WP and limited ORF27$^-$eGFP$^+$ infection.

(F) Mean ± SD. WP infection rates from three sections each of three mice per group. At day 8, ORF27$^-$ WP infection was significantly less than that of WT or revertant viruses ($p < 0.01$).

Institute) (Rickert et al., 1997) were infected with MuHV-4 when 6–12 weeks old, either i.n. in 30 μl under isoflurane anesthesia (10^4 p.f.u.) or i.p. in 100 μ1 (10^6 p.f.u.). CD19-cre disrupts CD19 (Rickert et al., 1997), so we used $CD19^{+/cre}$ mice for floxed virus tracking and $CD19^{cre/cre}$ mice as CD19 knockouts. Ai6-ZSgreen1 reporter mice (Madisen et al., 2010) were provided by S. Efstathiou (University of Cambridge, Cambridge, UK). For luciferase imaging, mice were given luciferin i.p. (2 mg/mouse) and scanned in an IVIS Lumina (Caliper Life Sciences). To empty the MZ of B cells, mice were injected i.p. with FTY720 (Cayman Chemical) (for i.p. infections, 2 mg/kg the day before and 1 mg/kg/day thereafter; for i.n. infections, 2 mg/kg on the day of infection and 1mg/kg every other day thereafter). All animal experiments were approved by the Cambridge University Ethical Review Board (Project License 80/2538).

Cells and Viruses

BHK-21 (American Type Culture Collection CCL-10), 3T3-CRE (Stevenson et al., 2002), and 3T3-ORF50 cells (Milho et al., 2009) were grown in Dulbecco's Modified Eagle's Medium, 2 mM glutamine, 100 U/ml penicillin, 100 μg/ml streptomycin, and 10% fetal calf serum. MHV-LUC, MHV-LoxP-eCFP (Gaspar et al., 2011), MHV-RG, and $ORF50^+$ (wild-type) (Frederico et al., 2012) and $ORF50^-$ (replication-deficient) (Milho et al., 2009) versions of EF1α-eGFP MuHV-4 have been described. ORF27-deficient (27^-FRT, 27^-STOP) and 27^-FRT revertant (27^+REV) BACs (May et al., 2005) were combined with the EF1α-eGFP reporter construct and virus recovered by transfecting BHK-21 cells. The BAC cassette was removed by virus passage through 3T3-CRE cells. $ORF50^-$ MuHV-4 was grown and titered on 3T3-ORF50 cells. Other viruses were grown and titered on BHK-21 cells. Virions were harvested from infected cell supernatants by ultracentrifugation (35,000 *g*, 90 min), and cell debris was removed by low-speed centrifugation (500 *g*, 5 min).

Infectivity Assays

Infectious virus was measured by plaque assay. Virus stocks or organ homogenates were incubated with BHK-21 cells (2 hr, 37°C), then overlaid with 0.3% carboxymethylcellulose. Four days later, the cells were fixed (4% formaldehyde) and stained (0.1% toluidine blue) for plaque counting. Latent plus infectious virus was measured by infectious center assay: single-cell suspensions of explanted spleens and LNs were cocultured with BHK-21 cells, then fixed and stained after 4 days. Infectious virus in lymphoid tissue is typically <5% of the total recoverable virus, so the infectious center assay measures mainly latency. To assay fluorochrome switching by MHV-RG or MHV-LoxP-eCFP, plaque and infectious center assays were performed at limiting dilution in 96-well plates (12–24 wells per dilution), and plaques scored as red, green, or eCFP fluorescent under ultraviolet illumination. Statistical comparisons were by Student's two-tailed unpaired t test.

Viral Genome Quantitation

MuHV-4 genomic coordinates 4166–4252 were amplified by PCR (Rotor Gene 3000, Corbett Research) from tissue DNA, quantitated by fluorescent probe hybridization (coordinates 4218–4189), and converted to genome copies by comparison with cloned DNA amplified in parallel. Cellular DNA was quantitated in the same reaction by amplifying part of the adenosine phosphoribosyl transferase gene, again with probe hybridization and template dilutions amplified in parallel. Viral DNA loads were then normalized by cellular DNA loads (Gaspar et al., 2011).

Immunohistochemistry

Organs were fixed in PBS/4% formaldehyde (24 hr, 4°C), dehydrated in 70% ethanol, and embedded in paraffin. Sections of 7 μm were de-waxed in xylene and hydrated in water/ethanol. Endogenous peroxidase activity was quenched in PBS/3% H_2O_2 (10 min, 23°C). Sections were blocked with Avidin/Biotin Blocking Kit (Vector Laboratories) and PBS/2% BSA/2% serum of the secondary antibody species (1 hr, 23°C). B cells were detected with anti-B220 (RA3-6B2, Abcam), RP macrophages with anti-F4/80 (Cl:A3-1), MZ macrophages with anti-CD169 (3D6.112, Serotec), and MuHV-4 with a rabbit pAb kindly provided by Dr. L. Gillet (University of Liège). After incubation with primary antibodies (16 hr, 23°C), sections were washed 3× in PBS, incubated with biotinylated rabbit anti-rat IgG pAb or biotinylated goat anti-rabbit IgG pAb (30 min, 23°C, Vector), washed 3× in PBS, incubated with Vectastain Elite ABC Peroxidase system (30 min, 23°C), washed 3× in PBS, and then incubated with ImmPACT DAB substrate (5min, 23°C, Vector). Sections were counterstained with Mayer's Hemalum, dehydrated in ethanol, and mounted in DPX.

Immunofluorescence

Organs were fixed in 1% formaldehyde/10 mM sodium periodate /75 mM L-lysine (24 hr, 4°C), equilibrated in 30% sucrose (18 hr, 4°C), and then frozen in OCT. Sections of 9 μm were air-dried (1 hr, 23°C), blocked with 0.3% Triton X-100/5% normal goat serum (1 hr, 23°C), and then incubated (18 hr, 4°C) with primary antibodies to eGFP (rabbit pAb, Abcam), mCherry (rabbit pAb, Badrilla), MARCO (ED31), MAdCAM-1 (MECA-367, Serotec), IgM (biotin-conjugated goat pAb), IgD (11-26c, Southern Biotech), CD1d (1B1), CR1/CR2 (7G6, BD Biosciences), or CD68 (FA-11, Biolegend). Antibodies to B220, CD169, F4/80, and MuHV-4 lytic antigens were as above. Sections were washed 3× in PBS, incubated (1 hr, 23°C) with Alexa633-conjugated goat anti-rat IgG pAb, streptavidin-conjugated Alexa568, and Alexa488- or 568-conjugated goat anti-rabbit IgG pAb (Invitrogen), washed 3× in PBS, and mounted in Prolong Gold + DAPI. Fluorescence was visualized with a Leica TCS SP5 confocal microscope and analyzed with ImageJ.

Flow Cytometry

Spleen cells were harvested from mice infected with $eGFP^+$ MuHV-4. IgG Fc receptor binding was blocked (30 min, 4°C) with rat anti-CD16/32 mAb before staining (1 hr, 4°C) with APC-conjugated anti-CD19, phycoerthyrin-conjugated anti-CD23, and biotinylated anti-CD35 (BD Biosciences). The cells were washed 2× in PBS, incubated (30 min, 4°C) with PerCP-conjugated streptavidin, washed 2× in PBS, and then analyzed on a FACS Calibur.

SUPPLEMENTAL INFORMATION

Supplemental Information includes three figures and can be found with this article online at http://dx.doi.org/10.1016/j.chom.2014.03.010.

ACKNOWLEDGMENTS

B.F. is supported by the Portuguese Foundation for Science and Technology, and B.C. by the Gates Foundation. This work was also supported by grants from the ARC (FT130100138), BBSRC (BB/J014419/1), NHMRC (637319, 1060138, 1064015), and Belspo (BelVir).

Received: June 30, 2013
Revised: December 5, 2013
Accepted: February 3, 2014
Published: April 9, 2014

REFERENCES

Arnon, T.I., Horton, R.M., Grigorova, I.L., and Cyster, J.G. (2013). Visualization of splenic marginal zone B-cell shuttling and follicular B-cell egress. Nature *493*, 684–688.

Barton, E., Mandal, P., and Speck, S.H. (2011). Pathogenesis and host control of gammaherpesviruses: lessons from the mouse. Annu. Rev. Immunol. *29*, 351–397.

Blackman, M.A., and Flaño, E. (2002). Persistent gamma-herpesvirus infections: what can we learn from an experimental mouse model? J. Exp. Med. *195*, F29–F32.

Borza, C.M., and Hutt-Fletcher, L.M. (2002). Alternate replication in B cells and epithelial cells switches tropism of Epstein-Barr virus. Nat. Med. *8*, 594–599.

Callan, M.F., Steven, N., Krausa, P., Wilson, J.D., Moss, P.A., Gillespie, G.M., Bell, J.I., Rickinson, A.B., and McMichael, A.J. (1996). Large clonal expansions of CD8+ T cells in acute infectious mononucleosis. Nat. Med. *2*, 906–911.

Carrasco, Y.R., and Batista, F.D. (2007). B cells acquire particulate antigen in a macrophage-rich area at the boundary between the follicle and the subcapsular sinus of the lymph node. Immunity *27*, 160–171.

Cerutti, A., Cols, M., and Puga, I. (2013). Marginal zone B cells: virtues of innate-like antibody-producing lymphocytes. Nat. Rev. Immunol. *13*, 118–132.

Chen, L.L., Frank, A.M., Adams, J.C., and Steinman, R.M. (1978). Distribution of horseradish peroxidase (HRP)-anti-HRP immune complexes in mouse spleen with special reference to follicular dendritic cells. J. Cell Biol. *79*, 184–199.

Chen, A., and Kaufman, S. (1996). Splenic blood flow and fluid efflux from the intravascular space in the rat. J. Physiol. *490*, 493–499.

Cinamon, G., Matloubian, M., Lesneski, M.J., Xu, Y., Low, C., Lu, T., Proia, R.L., and Cyster, J.G. (2004). Sphingosine 1-phosphate receptor 1 promotes B cell localization in the splenic marginal zone. Nat. Immunol. *5*, 713–720.

Clausen, B.E., Burkhardt, C., Reith, W., Renkawitz, R., and Förster, I. (1999). Conditional gene targeting in macrophages and granulocytes using LysMcre mice. Transgenic Res. *8*, 265–277.

Fehr, T., Rickert, R.C., Odermatt, B., Roes, J., Rajewsky, K., Hengartner, H., and Zinkernagel, R.M. (1998). Antiviral protection and germinal center formation, but impaired B cell memory in the absence of CD19. J. Exp. Med. *188*, 145–155.

Fooksman, D.R., Schwickert, T.A., Victora, G.D., Dustin, M.L., Nussenzweig, M.C., and Skokos, D. (2010). Development and migration of plasma cells in the mouse lymph node. Immunity *33*, 118–127.

François, S., Vidick, S., Sarlet, M., Desmecht, D., Drion, P., Stevenson, P.G., Vanderplasschen, A., and Gillet, L. (2013). Illumination of murine gammaherpesvirus-68 cycle reveals a sexual transmission route from females to males in laboratory mice. PLoS Pathog. *9*, e1003292.

Frederico, B., Milho, R., May, J.S., Gillet, L., and Stevenson, P.G. (2012). Myeloid infection links epithelial and B cell tropisms of Murid Herpesvirus-4. PLoS Pathog. *8*, e1002935.

Gan, Y.J., Sullivan, J.L., and Sixbey, J.W. (1994). Detection of cell-free Epstein-Barr virus DNA in serum during acute infectious mononucleosis. J. Infect. Dis. *170*, 436–439.

Ganem, D. (2006). KSHV infection and the pathogenesis of Kaposi's sarcoma. Annu. Rev. Pathol. *1*, 273–296.

Gaspar, M., May, J.S., Sukla, S., Frederico, B., Gill, M.B., Smith, C.M., Belz, G.T., and Stevenson, P.G. (2011). Murid herpesvirus-4 exploits dendritic cells to infect B cells. PLoS Pathog. *7*, e1002346.

George, L.C., Rowe, M., and Fox, C.P. (2012). Epstein-barr virus and the pathogenesis of T and NK lymphoma: a mystery unsolved. Curr. Hematol. Malig. Rep. *7*, 276–284.

Gill, M.B., Edgar, R., May, J.S., and Stevenson, P.G. (2008). A gamma-herpesvirus glycoprotein complex manipulates actin to promote viral spread. PLoS One *3*, e1808.

Gillet, L., May, J.S., Colaco, S., and Stevenson, P.G. (2007a). The murine gammaherpesvirus-68 gp150 acts as an immunogenic decoy to limit virion neutralization. PLoS ONE *2*, e705.

Gillet, L., May, J.S., and Stevenson, P.G. (2007b). Post-exposure vaccination improves gammaherpesvirus neutralization. PLoS ONE *2*, e899.

Gillet, L., Colaco, S., and Stevenson, P.G. (2008). Glycoprotein B switches conformation during murid herpesvirus 4 entry. J. Gen. Virol. *89*, 1352–1363.

Glauser, D.L., Kratz, A.S., and Stevenson, P.G. (2012). Herpesvirus glycoproteins undergo multiple antigenic changes before membrane fusion. PLoS ONE *7*, e30152.

Guerreiro-Cacais, A.O., Li, L., Donati, D., Bejarano, M.T., Morgan, A., Masucci, M.G., Hutt-Fletcher, L., and Levitsky, V. (2004). Capacity of Epstein-Barr virus to infect monocytes and inhibit their development into dendritic cells is affected by the cell type supporting virus replication. J. Gen. Virol. *85*, 2767–2778.

Hume, D.A. (2011). Applications of myeloid-specific promoters in transgenic mice support in vivo imaging and functional genomics but do not support the concept of distinct macrophage and dendritic cell lineages or roles in immunity. J. Leukoc. Biol. *89*, 525–538.

Junt, T., Moseman, E.A., Iannacone, M., Massberg, S., Lang, P.A., Boes, M., Fink, K., Henrickson, S.E., Shayakhmetov, D.M., Di Paolo, N.C., et al. (2007). Subcapsular sinus macrophages in lymph nodes clear lymph-borne viruses and present them to antiviral B cells. Nature *450*, 110–114.

Kurth, J., Spieker, T., Wustrow, J., Strickler, G.J., Hansmann, L.M., Rajewsky, K., and Küppers, R. (2000). EBV-infected B cells in infectious mononucleosis: viral strategies for spreading in the B cell compartment and establishing latency. Immunity *13*, 485–495.

Laichalk, L.L., and Thorley-Lawson, D.A. (2005). Terminal differentiation into plasma cells initiates the replicative cycle of Epstein-Barr virus in vivo. J. Virol. *79*, 1296–1307.

Liang, X., Collins, C.M., Mendel, J.B., Iwakoshi, N.N., and Speck, S.H. (2009). Gammaherpesvirus-driven plasma cell differentiation regulates virus reactivation from latently infected B lymphocytes. PLoS Pathog. *5*, e1000677.

Lopes-Carvalho, T., and Kearney, J.F. (2004). Development and selection of marginal zone B cells. Immunol. Rev. *197*, 192–205.

Madisen, L., Zwingman, T.A., Sunkin, S.M., Oh, S.W., Zariwala, H.A., Gu, H., Ng, L.L., Palmiter, R.D., Hawrylycz, M.J., Jones, A.R., et al. (2010). A robust and high-throughput Cre reporting and characterization system for the whole mouse brain. Nat. Neurosci. *13*, 133–140.

Makowska, A., Faizunnessa, N.N., Anderson, P., Midtvedt, T., and Cardell, S. (1999). CD1high B cells: a population of mixed origin. Eur. J. Immunol. *29*, 3285–3294.

Marques, S., Efstathiou, S., Smith, K.G., Haury, M., and Simas, J.P. (2003). Selective gene expression of latent murine gammaherpesvirus 68 in B lymphocytes. J. Virol. *77*, 7308–7318.

Martin, F., and Kearney, J.F. (2000). Positive selection from newly formed to marginal zone B cells depends on the rate of clonal production, CD19, and btk. Immunity *12*, 39–49.

May, J.S., Walker, J., Colaco, S., and Stevenson, P.G. (2005). The murine gammaherpesvirus 68 ORF27 gene product contributes to intercellular viral spread. J. Virol. *79*, 5059–5068.

Milho, R., Smith, C.M., Marques, S., Alenquer, M., May, J.S., Gillet, L., Gaspar, M., Efstathiou, S., Simas, J.P., and Stevenson, P.G. (2009). In vivo imaging of murid herpesvirus-4 infection. J. Gen. Virol. *90*, 21–32.

Milho, R., Frederico, B., Efstathiou, S., and Stevenson, P.G. (2012). A heparan-dependent herpesvirus targets the olfactory neuroepithelium for host entry. PLoS Pathog. *8*, e1002986.

Nash, A.A., and Sunil-Chandra, N.P. (1994). Interactions of the murine gammaherpesvirus with the immune system. Curr. Opin. Immunol. *6*, 560–563.

Phan, T.G., Green, J.A., Gray, E.E., Xu, Y., and Cyster, J.G. (2009). Immune complex relay by subcapsular sinus macrophages and noncognate B cells drives antibody affinity maturation. Nat. Immunol. *10*, 786–793.

Piguet, V., and Steinman, R.M. (2007). The interaction of HIV with dendritic cells: outcomes and pathways. Trends Immunol. *28*, 503–510.

Rickert, R.C., Roes, J., and Rajewsky, K. (1997). B lymphocyte-specific, Cre-mediated mutagenesis in mice. Nucleic Acids Res. *25*, 1317–1318.

Rosa, G.T., Gillet, L., Smith, C.M., de Lima, B.D., and Stevenson, P.G. (2007). IgG fc receptors provide an alternative infection route for murine gammaherpesvirus-68. PLoS ONE *2*, e560.

Sacher, T., Podlech, J., Mohr, C.A., Jordan, S., Ruzsics, Z., Reddehase, M.J., and Koszinowski, U.H. (2008). The major virus-producing cell type during murine cytomegalovirus infection, the hepatocyte, is not the source of virus dissemination in the host. Cell Host Microbe *3*, 263–272.

Savard, M., Bélanger, C., Tardif, M., Gourde, P., Flamand, L., and Gosselin, J. (2000). Infection of primary human monocytes by Epstein-Barr virus. J. Virol. *74*, 2612–2619.

Smith, C.M., Gill, M.B., May, J.S., and Stevenson, P.G. (2007). Murine gammaherpesvirus-68 inhibits antigen presentation by dendritic cells. PLoS ONE *2*, e1048.

Sokal, E.M., Hoppenbrouwers, K., Vandermeulen, C., Moutschen, M., Léonard, P., Moreels, A., Haumont, M., Bollen, A., Smets, F., and Denis, M. (2007). Recombinant gp350 vaccine for infectious mononucleosis: a phase 2, randomized, double-blind, placebo-controlled trial to evaluate the safety,

immunogenicity, and efficacy of an Epstein-Barr virus vaccine in healthy young adults. J. Infect. Dis. *196*, 1749–1753.

Steiniger, B., Barth, P., Herbst, B., Hartnell, A., and Crocker, P.R. (1997). The species-specific structure of microanatomical compartments in the human spleen: strongly sialoadhesin-positive macrophages occur in the perifollicular zone, but not in the marginal zone. Immunology *92*, 307–316.

Stevenson, P.G., Belz, G.T., Altman, J.D., and Doherty, P.C. (1999). Changing patterns of dominance in the CD8+ T cell response during acute and persistent murine gamma-herpesvirus infection. Eur. J. Immunol. *29*, 1059–1067.

Stevenson, P.G., May, J.S., Smith, X.G., Marques, S., Adler, H., Koszinowski, U.H., Simas, J.P., and Efstathiou, S. (2002). K3-mediated evasion of CD8(+) T cells aids amplification of a latent gamma-herpesvirus. Nat. Immunol. *3*, 733–740.

Stevenson, P.G., Simas, J.P., and Efstathiou, S. (2009). Immune control of mammalian gamma-herpesviruses: lessons from murid herpesvirus-4. J. Gen. Virol. *90*, 2317–2330.

Thorley-Lawson, D.A., Duca, K.A., and Shapiro, M. (2008). Epstein-Barr virus: a paradigm for persistent infection - for real and in virtual reality. Trends Immunol. *29*, 195–201.

Usherwood, E.J., Stewart, J.P., Robertson, K., Allen, D.J., and Nash, A.A. (1996). Absence of splenic latency in murine gammaherpesvirus 68-infected B cell-deficient mice. J. Gen. Virol. *77*, 2819–2825.

Valmary, S., Richard, P., and Brousset, P. (2005). Frequent detection of Kaposi's sarcoma herpesvirus in germinal centre macrophages from AIDS-related multicentric Castleman's disease. AIDS *19*, 1229–1231.

Walling, D.M., Ray, A.J., Nichols, J.E., Flaitz, C.M., and Nichols, C.M. (2007). Epstein-Barr virus infection of Langerhans cell precursors as a mechanism of oral epithelial entry, persistence, and reactivation. J. Virol. *81*, 7249–7268.

Weill, J.C., Weller, S., and Reynaud, C.A. (2009). Human marginal zone B cells. Annu. Rev. Immunol. *27*, 267–285.

Willer, D.O., and Speck, S.H. (2003). Long-term latent murine Gammaherpesvirus 68 infection is preferentially found within the surface immunoglobulin D-negative subset of splenic B cells in vivo. J. Virol. *77*, 8310–8321.

Xu, W., Santini, P.A., Sullivan, J.S., He, B., Shan, M., Ball, S.C., Dyer, W.B., Ketas, T.J., Chadburn, A., Cohen-Gould, L., et al. (2009). HIV-1 evades virus-specific IgG2 and IgA responses by targeting systemic and intestinal B cells via long-range intercellular conduits. Nat. Immunol. *10*, 1008–1017.